



American Society of  
Mechanical Engineers

## ASME Accepted Manuscript Repository

### Institutional Repository Cover Sheet

James

Zhan

*First*

*Last*

ASME Paper Title: Analytical Study of Coupling Effects for Vibrations of Cable-Harnessed Beam Structures

Authors: Karthik Yerrapragada, Armaghan Salehian

ASME Journal Title: Journal of Vibration and Acoustics

Volume/Issue 141/3

Date of Publication (VOR\* Online) January 22, 2019

ASME Digital Collection URL: <https://asmedigitalcollection.asme.org/vibrationacoustics/article/doi/10.1115/1.4042042>  
[ytical-Study-of-Coupling-Effects-for](#)

DOI: <https://doi.org/10.1115/1.4042042>

\*VOR (version of record)

# Analytical Study of Coupling Effects for Vibrations of Cable-Harnessed Beam Structures

**Karthik Yerrapragada**

PhD Candidate

Department of Mechanical and Mechatronics  
Engineering

University of Waterloo

Waterloo, Ontario, CANADA, N2L 3G1

email: [kyerrapr@uwaterloo.ca](mailto:kyerrapr@uwaterloo.ca)

**Armaghan Salehian\***

Associate Professor

Department of Mechanical and Mechatronics  
Engineering

University of Waterloo

Waterloo, Ontario, CANADA, N2L 3G1

email: [salehian@uwaterloo.ca](mailto:salehian@uwaterloo.ca)

## Abstract

This paper presents a distributed parameter model to study the effects of the harnessing cables on the dynamics of a host structure motivated by space structures applications. The structure is modeled using both Euler-Bernoulli and Timoshenko beam theories. The presented model studies the effects of coupling between various coordinates of vibrations due to the addition of the cable. The effects of the cable's offset position, pre-tension and radius are studied on the natural frequencies of the system. Strain and kinetic energy expressions using linear displacement field assumptions and Green-Lagrange strain tensor are developed. The governing coupled partial differential equations for the cable-harnessed beam that includes the effects of the cable pre-tension are found using Hamilton's principle. The natural frequencies from the coupled Euler Bernoulli, Timoshenko and decoupled analytical models are found and compared to the results of the Finite Element Analysis.

**Keywords:** Beam Structures, Cable-Harnessed Structures, Coupled Vibration Analysis, Tension.

## Nomenclature

$u(x, t)$	Axial displacement
$v(x, t)$	In plane bending displacement
$w(x, t)$	Out of plane bending displacement
$\theta(x, t)$	Torsional displacement
$\varphi(x, t)$	Rotation of cross-section about z axis
$\psi(x, t)$	Rotation of cross-section about y axis
$\nu$	Poisson's Ratio
$\kappa$	Shear Correction Factor
$E_b$	Young's Modulus of the beam
$G_b$	Shear Modulus of the beam
$A_b$	Area of cross section of the beam
$A_c$	Area of cross section of the cable
$E_c$	Young's modulus of the cable
$b_1 - b_9$	Strain energy coefficients of Euler Bernoulli model
$c_1 - c_{15}$	Strain energy coefficients of Timoshenko model
$k_1 - k_6$	Kinetic energy coefficients

$\omega$	Natural Frequency
$\omega_f$	Driving frequency
$x_s$	Sensing location
$x_a$	Actuation location
$(\epsilon_{xx})_b$	Direct strain in the beam in the x direction
$(\epsilon_{xx})_c$	Direct strain in the cable in the x-direction
$(\gamma_{xy})_b$	Shear strain in the beam in the xy plane
$(\gamma_{xz})_b$	Shear strain in the beam in the xz plane
$\rho_b$	Density of the beam
$\rho_c$	Density of the cable
$l$	Length of the beam
$b$	Width of the beam
$h$	Depth of the beam
$T$	Pre-tension of the cable
$r_c$	Radius of the cable
$y_c$	y coordinate of the center of the cable ( $y_c = \frac{b}{2} - r_c$ )
$z_c$	z coordinate of the center of the cable ( $z_c = \frac{h}{2} + r_c$ )
$A_c$	Area of cross-section of the cable ( $A_c = \pi r_c^2$ ), circular cross-section
$A_b$	Area of cross-section of the beam

## 1. Introduction

Large space structures are often too large for dynamic ground testing as a whole. Therefore, a common approach to model validations for these structures entails ground testing the individual components prior to their launch. One major component for these structures include electronic cords and power cables that have been commonly ignored in modeling these structures. These cables have shown to weigh up to 20% of the mass of the host structure [1]. This number will increase significantly with the use of composite materials in aerospace applications. Therefore, obtaining a dynamic model that accurately accounts for the mass, stiffness and damping effects of these cables is of paramount importance and has received a lot of attention in the past few years [2,3]. Apart from space structures, cables also have important structural applications in the areas of (but not limited to) power lines and marine applications. In power lines [4] stranded cables are used frequently, where several wires are twisted to form a single cable. Ref. [4] models the dynamic response of power transmission cables when subjected to shock loads. The stranded cables considered in [4] comprise of aluminum and galvanized steel. Ref. [5] develops mathematical models to determine the bending stiffness of stranded cables which have application in power and signal transmission. In marine cables [6] two layers are present. Armour layer is the outer, which provides the mechanical strength, and the inner layer contains optical fibers and conducting wires [6]. Ref. [7] states that the marine cables usually cannot withstand compressive load and operate in tension-slack condition which results in non-linear behaviour. In space structure applications, the power cables are attached to the host structures using zip-ties and the cable resonances are usually observed in the higher modes and the presence

of cabling significantly effects the dynamics of the host structure [2]. In the current paper, the pre-tensioned cable is attached all along the length of the beam (host structure). Cabling induces coupled vibration behaviour between various coordinates and this phenomenon is investigated analytically in this work. For the cable model in this paper, the strain and kinetic energy expressions are evaluated based on the strain and displacement values at the centre of the cable cross-section.

Previous research in the area of cable-harnessed structures includes ad hoc techniques that mathematically model these cables as lumped masses attached to the host structure ignoring their stiffness and damping properties [8] . To overcome deficiencies in the earlier models, [1] considers the effect of distributed mass, stiffness and damping effects of cables where added cables are modeled as a beam structure attached to a host specimen. Ref. [1] models the cables using shear-beam theory. The dynamics of cabled beam is studied using analytical methods. The paper reports bending modes related to the host structure and the cable. It is reported that the shear beam model (for cable) predicts damping better than the case where the cable is modelled using Euler-Bernoulli beam model. Goodding et al [3,9] developed methods to attach the cable to the host structures with the help of tie-down structures. The paper reports that at lower modes, mass effects dominate and at higher modes, the damping effects increase. Their work pertains to studying bending vibrations using finite element analysis (FEA) for free-free cabled structures. The bending frequency response functions obtained from the FEA are validated using experiments. Babuska et al [2] model the host structure and cable using Euler-Bernoulli beam theory. They develop distributed parameter model for transverse vibrations of cable and beam. It is also shown in their work that the stiffness effects are dominant in the lower vibration modes, where as, the damping effects dominate the higher modes of vibrations. Refs. [10] develop a cable loaded panel. The host structure considered is a plate and cables are attached to it. The paper develops finite element model to predict the vibration characteristics of the cable loaded panel and the finite element model is validated with experiments.

Spak et. al Refs. [5,11–13] modeled the spaceflight cables using the shear and Timoshenko beam theory and developed theoretical models to determine various effective properties of non-homogenous space flight cables such as density and Young's modulus. Using the predicted properties, the frequency response characteristics of bending vibrations cable harnessed structures are found out using analytical methods and the predicted frequency response functions are validated using experiments. The initial phase of Spak et al work studies the frequency response of strings and space flight cables. The experimental investigations in Ref. [14] study the bending vibration characteristics of cables (modeled as beams). Spak et al report that as the tension in string and cables vary, the structure's frequency response shifts slightly. The paper validated the cable models for bending modes that are developed using beam theory (model solved using DTFM approach) with the experiments. Extensive experimental investigations in [13] focuses on cabled beams and reports the existence of cable-beam interaction modes and coupled bending-torsion

modes. Spak et al report that when host structure is harnessed with thick space flight cables, the presence of interaction and torsional modes is seen experimentally. The analytical model by Ref.[13] neglects the effect of bending torsional coupling in the cabled structure. Ref. [13] compares the analytical model's bending frequency response function with that of experimental frequency response function.

Choi et. al [15] model both the bending vibrations of cable and beam structures using Timoshenko beam theory. The cable is attached to the beam using tie down structures. The frequency response functions for the bending mode obtained using the Spectral Element Method are compared with the Finite Element Method (FEM). Authors [15] conclude that Spectral Element Method uses significantly lower number of elements when compared to the FEM method. Huang et al [16,17] extend this spectral element approach developed by Choi et al [15] to study the bending vibration characteristics of a cantilevered cable-harnessed beam with a tip mass at the free end. The mathematical model [16,17] also accounts for damping in the structure part from extensively studying of tip mass.

Martin et al [18–23] developed analytical models along with their experimental validations for cable-harnessed beam structures of periodic cable patterns. In their work, cables are modeled using both bar and string element assumptions. Partial Differential Equations (PDEs) that account for cables' mass, stiffness and tension properties on the system's dynamics are developed. In all the developed models in [18–23], the out-of-plane bending is of primary interest. The method used employs the homogenization technique for truss structures in [24–29] to obtain the PDE's using a linear displacement field through the strain and kinetic energy expressions of a fundamental repeated elements. The coupling induced between various coordinates of vibrations due to the addition of the cables is entirely neglected in their modelling.

Therefore, a main object of the current work is to extend the studies in [18–23] to investigate the effects of coupling induced in the system due to presence of the cables on the host structure. As this paper represents the first attempt by the authors on the coupled vibrations analysis for cable harnessed beams, a simpler pattern geometry for the cable is considered for the current work compared to the previously published work by Martin et. al [18–23]. The presented work extends the assumptions of the model that is previously used to study uni-dimensional vibrations in the out-of-plane bending direction to account for the coupling between various coordinates of vibrations such as in-plane bending, out-of-plane bending, torsion and the axial modes. Both Euler Bernoulli (EB) and Timoshenko beam theories (TBT) are used. The effects of several cable parameters such as the cable offset position, radius and pre-tension on the system's coupled dynamics are investigated. The results are compared to a decoupled model to indicate the importance of including the coupling effects into the system's dynamics.

The paper is organized as follows, in section 2, the system's configuration, the developed mathematical model for the fully coupled cable-harnessed beam and the procedure to find out the natural frequencies are presented. In section 3, the natural frequencies for the decoupled and coupled vibration

models are compared to the finite element results for several boundary conditions such as the fixed-fixed, cantilever and simply supported. Finally, the results for the sensitivity analysis to study the effects of several cable parameters such as cable's geometry, pre-tension and offset position on the natural frequencies are presented. The relation between the system's coupling and the energy transfer between various coordinates of vibrations are also studied. The frequency response functions when the structure is excited in the out of plane bending direction for cantilever boundary condition is also presented.

## 2. Mathematical Modeling

This section presents the mathematical modeling and underlying assumptions for the structure in this study. The structure considered is a beam system with a cable attached along the side of the beam as shown in Figure (1). The coordinate axes are shown in the figure. The cable is positioned at an offset distance along the y-axis.

To develop the continuum model of the cable-harnessed structure, the following assumptions apply:

- 1) The host structure is assumed to be a beam and it is modeled using Euler-Bernoulli and Timoshenko beam theories.
- 2) The cable stays in contact with the beam during vibrations along its length. This is because the electronic cords and power cables are secured in place using cable ties that prevents them from being detached from the host structure during vibrations.
- 3) The strain values at a cable cross-section remains the same as the values evaluated at the center of the cable cross-section due to its radius being small.
- 4) The cable is in pre-tension at the equilibrium position and will remain in tension during the vibrations. The tension value is assumed to be constant during vibrations.
- 5) The pre-tension in the cable results in the pre-compression in the beam [23].

The following sections pertain to the free vibration analysis of the cable-harnessed beam shown in Figure (1) using a distributed parameter model. The previous work by the authors on the analytical model for the periodically wrapped beam, [23], excludes the coupling effects between various coordinates of vibrations, i.e., bending, axial and torsion. The following steps outline the procedure for a fully coupled continuum model development for the system shown in Figure (1) using Euler-Bernoulli and Timoshenko beam theories. The first step in finding an equivalent continuum model is to establish the displacement field relationship and stress-strain components. The linearized three-dimensional displacement fields using Euler-Bernoulli (EB) and Timoshenko beam theories are as follows [30–33].

### Euler-Bernoulli beam model

$$X(x, y, z, t) = u(x, t) - y \frac{\partial v(x, t)}{\partial x} - z \frac{\partial w(x, t)}{\partial x}$$

$$Y(x, y, z, t) = v(x, t) - z\theta(x, t)$$

$$Z(x, y, z, t) = w(x, t) + y\theta(x, t)$$

### Timoshenko beam model

$$X(x, y, z, t) = u(x, t) - y\varphi(x, t) + z\psi(x, t)$$

$$Y(x, y, z, t) = v(x, t) - z\theta(x, t)$$

$$Z(x, y, z, t) = w(x, t) + y\theta(x, t)$$

(1)

where  $u(x, t)$ ,  $v(x, t)$ ,  $w(x, t)$ ,  $\theta(x, t)$ ,  $\varphi(x, t)$ ,  $\psi(x, t)$  are the motions in the axial, in-plane bending, out-of-plane bending, torsion, rotation of cross-section about z and y-axes respectively. The next step is to find the stress-strain expressions using the displacement field. Equation (2) gives the relationship between the stress and strain for an isotropic material.

$$\begin{Bmatrix} \sigma_{xx} \\ \sigma_{yy} \\ \sigma_{zz} \\ \tau_{xy} \\ \tau_{yz} \\ \tau_{zx} \end{Bmatrix} = \begin{bmatrix} \frac{E(1-\nu)}{(1+\nu)(1-2\nu)} & \frac{E\nu}{(1+\nu)(1-2\nu)} & \frac{E\nu}{(1+\nu)(1-2\nu)} & 0 & 0 & 0 \\ \frac{E\nu}{(1+\nu)(1-2\nu)} & \frac{E(1-\nu)}{(1+\nu)(1-2\nu)} & \frac{E\nu}{(1+\nu)(1-2\nu)} & 0 & 0 & 0 \\ \frac{E\nu}{(1+\nu)(1-2\nu)} & \frac{E\nu}{(1+\nu)(1-2\nu)} & \frac{E(1-\nu)}{(1+\nu)(1-2\nu)} & 0 & 0 & 0 \\ \frac{E\nu}{(1+\nu)(1-2\nu)} & \frac{E\nu}{(1+\nu)(1-2\nu)} & \frac{E(1-\nu)}{(1+\nu)(1-2\nu)} & 0 & 0 & 0 \\ 0 & 0 & 0 & G & 0 & 0 \\ 0 & 0 & 0 & 0 & G & 0 \\ 0 & 0 & 0 & 0 & 0 & G \end{bmatrix} \begin{Bmatrix} \varepsilon_{xx} \\ \varepsilon_{yy} \\ \varepsilon_{zz} \\ \gamma_{xy} \\ \gamma_{yz} \\ \gamma_{zx} \end{Bmatrix} \quad (2)$$

[D]

where [D] is the elasticity matrix, and  $E$  and  $G$  are the Young's and the Shear Moduli respectively. The expressions for the Green-Lagrange strain tensor are shown in Equations. (3-5) [30,33]. This structure is modelled using beam theory, therefore, the strain components in the y and z directions, ( $\varepsilon_{yy}$  and  $\varepsilon_{zz}$ ), and the shear strain on the yz plane, ( $\gamma_{yz}$ ), can be neglected (Ref. [30]). Once the continuum model based on the Timoshenko beam theory is obtained, the Euler-Bernoulli model can be obtained by neglecting the effects of shear deformation and rotary inertia [30,33].

$$\begin{aligned} \varepsilon_{xx} &= \frac{\partial X}{\partial x} + \frac{1}{2} \left( \frac{\partial X}{\partial x} \right)^2 + \frac{1}{2} \left( \frac{\partial Y}{\partial x} \right)^2 + \frac{1}{2} \left( \frac{\partial Z}{\partial x} \right)^2 \\ &= \left( \frac{\partial u}{\partial x} - y \frac{\partial \varphi}{\partial x} + z \frac{\partial \psi}{\partial x} \right) + \frac{1}{2} \left[ \left( \frac{\partial u}{\partial x} - y \frac{\partial \varphi}{\partial x} + z \frac{\partial \psi}{\partial x} \right)^2 + \left( \frac{\partial v}{\partial x} - z \frac{\partial \theta}{\partial x} \right)^2 + \left( \frac{\partial w}{\partial x} + y \frac{\partial \theta}{\partial x} \right)^2 \right] \end{aligned} \quad (3)$$

$$\begin{aligned} \gamma_{xy} &= \frac{\partial X}{\partial y} + \frac{\partial Y}{\partial x} + \frac{\partial X}{\partial x} \frac{\partial X}{\partial y} + \frac{\partial Y}{\partial x} \frac{\partial Y}{\partial y} + \frac{\partial Z}{\partial x} \frac{\partial Z}{\partial y} \\ &= -\sqrt{\kappa} \varphi + \sqrt{\kappa} \frac{\partial v}{\partial x} - z \frac{\partial \theta}{\partial x} \end{aligned} \quad (4)$$

$$\begin{aligned}\gamma_{zx} &= \frac{\partial Z}{\partial x} + \frac{\partial X}{\partial z} + \frac{\partial X}{\partial z} \frac{\partial X}{\partial x} + \frac{\partial Y}{\partial z} \frac{\partial Y}{\partial x} + \frac{\partial Z}{\partial z} \frac{\partial Z}{\partial x} \\ &= \sqrt{\kappa}\psi + \sqrt{\kappa} \frac{\partial w}{\partial x} + y \frac{\partial \theta}{\partial x}\end{aligned}\quad (5)$$

Here,  $\kappa$  is the shear correction factor and can be found as  $\frac{5+5\nu}{6+5\nu}$ , [33], where,  $\nu$  is the Poisson's ratio. The effect of Poisson's ratio on the direct strains of the host structure is neglected. The total strain energy of the unit can be found using the strain energy for each of the beam and cable as,

$$U = \frac{1}{2} \left[ \iiint \{\varepsilon\}_b^T \{\sigma\}_b dV + \iiint \{\varepsilon\}_c^T \{\sigma\}_c dV \right] \quad (6)$$

where  $\{\varepsilon\}_b$  and  $\{\varepsilon\}_c$  are the strain components of the beam and cable respectively.  $\{\sigma\}_b = [D]_b \{\varepsilon\}_b$  and  $\{\sigma\}_c = [D]_c \{\varepsilon\}_c$ . After neglecting  $\varepsilon_{yy}$ ,  $\varepsilon_{zz}$ ,  $\gamma_{yz}$  in Equation. (2) due to using a beam theory, the stresses in the beam are found using  $\{\sigma_{xx}, \tau_{xy}, \tau_{zx}\}_b^T = \{E_b(\varepsilon_{xx})_b, G_b(\gamma_{xy})_b, G_b(\gamma_{zx})_b\}^T$ . The cable is assumed to undergo strain in the  $x$  direction only, therefore,  $(\sigma_{xx})_c = E_c(\varepsilon_{xx})_c$ . Also, the shear modulus effects in the cable are assumed to be negligible. Additionally, the strains components for the beam and cable include the strain experienced during the vibrations as well as the cable pretension that also induces a pre-compression in the beam. Therefore, the expressions for the direct strains induced in the cable and beam after the incorporating the effect of pre-tension in the cable and pre-compression in the beam are as  $(\varepsilon_{xx})_c = T/E_c A_c + \varepsilon_{xx}$  and  $(\varepsilon_{xx})_b = -T/E_b A_b + \varepsilon_{xx}$ . The negative sign in the equation for  $(\varepsilon_{xx})_b$  is due to the pre-compression induced in the beam upon the cable pre-tension. The final energy expressions for the kinetic and strain of the cable-harnessed beam for a Timoshenko beam theory are as follows.

$$\begin{aligned}U_{system} &= \frac{1}{2} \left[ \iiint E_b(\varepsilon_{xx})_b^2 + G_b(\gamma_{xy})_b^2 + G_b(\gamma_{zx})_b^2 dV \right] + \frac{1}{2} \left[ \iiint E_c(\varepsilon_{xx})_c^2 dV \right] \\ &= \frac{1}{2} \int_0^l [c_1(u')^2 + c_2(v')^2 + c_3(w')^2 + c_4(\theta')^2 + c_5(\varphi')^2 + c_6(\psi')^2 + c_7(\varphi)^2 + \\ &2c_8(u')(\varphi') + 2c_9(u')(\psi') + 2c_{10}(\varphi')(\psi') + 2c_{11}(v')(\varphi) + 2c_{12}(v')(\theta') + 2c_{13}(w')(\theta') + \\ &c_{14}(\psi)^2 + 2c_{15}(w')(\psi)] dx\end{aligned}\quad (7)$$

$$\begin{aligned}T_{system} &= \frac{1}{2} \left[ \iiint \rho_{beam} \{\dot{X}, \dot{Y}, \dot{Z}\}^T \{\dot{X}, \dot{Y}, \dot{Z}\} dV + \iiint \rho_{cable} \{\dot{X}, \dot{Y}, \dot{Z}\}^T \{\dot{X}, \dot{Y}, \dot{Z}\} dV \right] \\ &= \frac{1}{2} \int_0^l [k_1(\dot{u})^2 + k_2(\dot{v})^2 + k_3(\dot{w})^2 + k_4(\dot{\theta})^2 + k_5(\dot{\varphi})^2 + k_6(\dot{\psi})^2] dx\end{aligned}\quad (8)$$

The constants used in the kinetic and strain energy expressions are as follows:

$$\begin{aligned}
c_1 &= E_b A_b + E_c A_c & c_{12} &= -z_c T \\
c_2 &= \kappa A_b G_b & c_{13} &= y_c T \\
c_3 &= \kappa A_b G_b & c_{14} &= \kappa A_b G_b \\
c_4 &= G_b J + T(y_c^2 + z_c^2) - \frac{TJ}{A_b} & c_{15} &= \kappa A_b G_b \\
c_5 &= E_c A_c y_c^2 + T y_c^2 + E_b I_{zz} - \frac{T I_{zz}}{A_b} & k_1 &= \rho_b A_b + \rho_c A_c \\
c_6 &= E_c A_c z_c^2 + T z_c^2 + E_b I_{yy} - \frac{T I_{yy}}{A_b} & k_2 &= \rho_b A_b + \rho_c A_c \\
c_7 &= \kappa A_b G_b & k_3 &= \rho_b A_b + \rho_c A_c \\
c_8 &= -E_c A_c y_c - T y_c & k_4 &= \rho_b I_{xx} + \rho_c A_c (y_c^2 + z_c^2) \\
c_9 &= E_c A_c z_c + T z_c & k_5 &= \rho_b I_{zz} + \rho_c A_c (y_c^2) \\
c_{10} &= (E_c A_c + T)(-y_c z_c) & k_6 &= \rho_b I_{yy} + \rho_c A_c (z_c^2) \\
c_{11} &= -\kappa A_b G_b & &
\end{aligned} \tag{9}$$

where,  $y_c$  and  $z_c$  are the position coordinates of the cable.  $I_{zz}$  and  $I_{yy}$  are the area moment of inertias of the beam about z-axis and y-axis respectively,  $J$  is the torsion constant of the beam,  $I_{xx} = I_{yy} + I_{zz}$  is the polar moment of inertia of the beam. Other parameters are defined in the nomenclature table.

The terms  $c_1$ ,  $c_2$ ,  $c_3$  and  $c_4$  represent the strain energies in the axial, in-plane bending, out of plane bending and torsion modes respectively.  $c_5$ ,  $c_7$  and  $c_6$ ,  $c_{14}$  represent the coefficients related to the two rotations of cross-sections. The remaining strain energy coefficients are due to coupling terms, which in case of Timoshenko model depend on the geometry and material properties of the host structure and the radius, pre-tension and position coordinates of the center of the cable.

The energy expressions for Euler-Bernoulli model can be found by neglecting shear deformation and rotary inertia effects. Assuming negligible initial twist, and zero wrapping angle of the cable, the strain and kinetic energy expressions of the system using this theory are found as Ref. [23],

$$U = \frac{1}{2} \int_0^l [b_1(u')^2 + b_2(v'')^2 + b_3(w'')^2 + b_4(\theta')^2 + 2b_5(v'')(w'') + 2b_6(u')(v'') \tag{10}$$

$$+ 2b_7(u')(w'') + 2b_8(w')( \theta') + 2b_9(v')( \theta')] dx$$

$$T = \frac{1}{2} \int_0^l [k_1(\dot{u})^2 + k_2(\dot{v})^2 + k_3(\dot{w})^2 + k_4(\dot{\theta})^2] dx \tag{11}$$

where superscript  $(\cdot)$  denotes partial derivative with respect to spatial coordinate  $x(\frac{\partial}{\partial x})$  and superscript  $(\dot{\cdot})$  denotes partial derivative with respect to time  $t(\frac{\partial}{\partial t})$ . The constants of the above strain and kinetic energy expressions are as follows:

$$\begin{aligned}
b_1 &= E_b A_b + E_c A_c & b_8 &= T y_c \\
b_2 &= E_b I_{zz} + E_c A_c y_c^2 + T y_c^2 - \frac{T I_{zz}}{A_b} & b_9 &= -T z_c \\
b_3 &= E_b I_{yy} + E_c A_c z_c^2 + T z_c^2 - \frac{T I_{yy}}{A_b} & k_1 &= \rho_b A_b + \rho_c A_c \\
b_4 &= G_b J + T(y_c^2 + z_c^2) - \frac{TJ}{A_b} & k_2 &= \rho_b A_b + \rho_c A_c \\
b_5 &= E_c A_c y_c z_c + T y_c z_c & k_3 &= \rho_b A_b + \rho_c A_c \\
b_6 &= (E_c A_c + T)(-y_c) & k_4 &= \rho_b I_{xx} + \rho_c A_c (y_c^2 + z_c^2) \\
b_7 &= (E_c A_c + T)(-z_c) & &
\end{aligned} \tag{12}$$

Here,  $b_1$  to  $b_4$  represent the coupling coefficients in the axial, in-plane bending, out-of-plane bending and torsion modes respectively. The remaining coefficients ( $b_5$  to  $b_9$ ) represent the coupling coefficients. The coupling coefficients in case of Euler-Bernoulli model depends on the parameters like cable radius, cable pre-tension, young's modulus of the cable and the position coordinates of the center of the cable along the y and z axis. Assuming free vibrations and no external loads acting on the system, equations of motion for free vibrations for the two beam theories may be found.

The coupled equations of motion for the six coordinates of vibrations for the Timoshenko beam model are found as,

$$-k_1 \ddot{u} + c_1 u'' + c_8 \varphi'' + c_9 \psi'' = 0 \tag{13a}$$

$$-k_2 \ddot{v} + c_2 v'' + c_{12} \theta'' + c_{11} \varphi' = 0 \tag{13b}$$

$$-k_3 \ddot{w} + c_3 w'' + c_{13} \theta'' + c_{15} \psi' = 0 \tag{13c}$$

$$-k_4 \ddot{\theta} + c_4 \theta'' + c_{12} v'' + c_{13} w'' = 0 \tag{13d}$$

$$-k_5 \ddot{\varphi} + c_5 \varphi'' - c_7 \varphi + c_8 u'' - c_{11} v' + c_{10} \psi'' = 0 \tag{13e}$$

$$-k_6 \ddot{\psi} + c_6 \psi'' - c_{14} \psi + c_9 u'' - c_{15} w' + c_{10} \varphi'' = 0 \tag{13f}$$

The six coupled partial differential equations obtained after applying Hamilton's principle are presented in Equations. (13a) - (13f) will require six boundary conditions at each end. The boundary conditions (also obtained from Hamilton's principle) for each of the fixed, simply supported and free ends are as follows. The boundary conditions for the fixed, free and simply supported ends are shown in Equations (14), (15) and (16) respectively.

$$u = v = w = \theta = \varphi = \psi = 0|_{x=0 \text{ or } l} \quad (14)$$

$$\begin{aligned} c_1 u' + c_8 \varphi' + c_9 \psi' &= 0|_{x=0 \text{ or } l} \\ c_2 v' + c_{11} \varphi + c_{12} \theta' &= 0|_{x=0 \text{ or } l} \\ c_3 w' + c_4 \theta' + c_{15} \psi &= 0|_{x=0 \text{ or } l} \\ c_4 \theta' + c_{12} v' + c_{13} w' &= 0|_{x=0 \text{ or } l} \\ c_5 \varphi' + c_8 u' + c_{10} \psi' &= 0|_{x=0 \text{ or } l} \\ c_6 \psi' + c_9 u' + c_{10} \varphi' &= 0|_{x=0 \text{ or } l} \end{aligned} \quad (15)$$

$$\begin{aligned} u = v = w = \theta &= 0|_{x=0 \text{ or } l} \\ c_5 \varphi' + c_8 u' + c_{10} \psi' &= 0|_{x=0 \text{ or } l} \\ c_6 \psi' + c_9 u' + c_{10} \varphi' &= 0|_{x=0 \text{ or } l} \end{aligned} \quad (16)$$

A simpler version of Equations. (13a) - (13f) can be found using assumptions for a Euler Bernoulli beam model in which the shear and rotary inertia effects are excluded. The governing equations for Euler Bernoulli beam model is presented in Equations. (17a)- (17d).

$$-k_1 \ddot{u} + b_1 u'' + b_6 v'''' + b_7 w'''' = 0 \quad (17a)$$

$$-k_2 \ddot{v} - b_2 v'''' - b_6 u'''' - b_5 w'''' + b_9 \theta'' = 0 \quad (17b)$$

$$-k_3 \ddot{w} - b_3 w'''' - b_7 u'''' - b_5 v'''' + b_8 \theta'' = 0 \quad (17c)$$

$$-k_4 \ddot{\theta} + b_4 \theta'' + b_9 v'' + b_8 w'' = 0 \quad (17d)$$

The associated boundary conditions for the Equations. (17a) - (17d) for the fixed, free and simply supported ends are shown in Equations (18), (19) and (20) respectively.

$$u = v = w = \theta = v' = w' = 0|_{x=0 \text{ or } l} \quad (18)$$

$$\begin{aligned} b_1 u' + b_6 v'' + b_7 w'' &= 0|_{x=0 \text{ or } l} \\ b_2 v'' + b_5 w'' + b_6 u' &= 0|_{x=0 \text{ or } l} \\ b_2 v'''' + b_5 w'''' + b_6 u'' - b_9 \theta' &= 0|_{x=0 \text{ or } l} \\ b_3 w'' + b_5 v'' + b_7 u' &= 0|_{x=0 \text{ or } l} \\ b_3 w'''' + b_5 v'''' + b_7 u'' - b_8 \theta' &= 0|_{x=0 \text{ or } l} \\ b_4 \theta' + b_8 w' + b_9 v' &= 0|_{x=0 \text{ or } l} \end{aligned} \quad (19)$$

$$\begin{aligned} u = v = w = \theta &= 0|_{x=0 \text{ or } l} \\ b_2 v'' + b_5 w'' + b_6 u' &= 0|_{x=0 \text{ or } l} \\ b_3 w'' + b_5 v'' + b_7 u' &= 0|_{x=0 \text{ or } l} \end{aligned} \quad (20)$$

For physical description of the governing coupled partial differential equations, Equations. (13a) - (13f) and Equations. (17a) - (17d), the readers can refer to section S1 in the supplementary document. After obtaining the governing equations, the next step is to obtain the natural frequencies and mode shapes. In the following steps, the solution procedure for coupled partial differential equations, the Timoshenko model is shown in Equations. (13a)- (13f). The same procedure is applicable for the Euler-Bernoulli model which are shown in Equations. (17a) - (17d). The general form of the solution for the coupled PDE's shown in Equations. (13a)- (13f) are as follows,

$$\begin{Bmatrix} u \\ v \\ w \\ \theta \\ \varphi \\ \psi \end{Bmatrix} = \begin{Bmatrix} U \\ V \\ W \\ \Theta \\ \Phi \\ \Psi \end{Bmatrix} e^{\alpha x} e^{i\omega t} \quad (21)$$

where  $U, V, W, \Theta, \Phi$  and  $\Psi$  are modal vectors. The temporal solution of the PDEs is assumed to be harmonic (represented by the complex exponential  $e^{i\omega t}$ ), and the spatial solution is assumed to be of the form  $e^{\alpha x}$ , where  $\omega$  is the frequency and  $\alpha$  is the mode shape parameter. Substituting Equation. (21) in Equations. (13a)- (13f), we obtain six simultaneous algebraic equations, which are converted into matrix form as follows,

$$[A]_{6 \times 6} \begin{Bmatrix} U \\ V \\ W \\ \Theta \\ \Phi \\ \Psi \end{Bmatrix}_{6 \times 1} = \{0\}_{6 \times 1} \quad (22)$$

where  $[A]$  is given by:

$$\begin{bmatrix} c_1\alpha^2 + k_1\omega^2 & 0 & 0 & 0 & c_8\alpha^2 & c_9\alpha^2 \\ 0 & c_2\alpha^2 + k_2\omega^2 & 0 & c_{12}\alpha^2 & c_{11}\alpha & 0 \\ 0 & 0 & c_3\alpha^2 + k_3\omega^2 & c_{13}\alpha^2 & 0 & c_{15}\alpha \\ 0 & c_{12}\alpha^2 & c_{13}\alpha^2 & c_4\alpha^2 + k_4\omega^2 & 0 & 0 \\ c_8\alpha^2 & -c_{11}\alpha & 0 & 0 & c_5\alpha^2 - c_7 + k_5\omega^2 & c_{10}\alpha^2 \\ c_9\alpha^2 & 0 & -c_{15}\alpha & 0 & c_{10}\alpha^2 & c_6\alpha^2 + k_6\omega^2 - c_{14} \end{bmatrix}$$

For non-trivial solution,  $|A(\alpha, \omega)|$  should be zero. This results in a polynomial that relates the mode shape parameters  $\alpha$  and frequency  $\omega$ . Solving the above polynomial results in 12 roots for  $\alpha$  in terms of  $\omega$ . The next step is to find the spatial solutions. We know from Equation. (22) that

$$A_{61}U + A_{62}V + A_{63}W + A_{64}\Theta + A_{65}\Phi + A_{66}\Psi = 0 \quad (23)$$

where  $A_{6i}$  ( $i \rightarrow 1$  to  $6$ ) represent the elements of the sixth row of matrix  $[A]$  (any arbitrary row can be used to develop the linear dependency condition. In this case, sixth row was selected). For the linear dependency between  $U, V, W, \Theta, \Phi$  and  $\Psi$  to be satisfied, the spatial solutions for different coordinates of motion should be as follows.

$$U_n = |(-1)^{6+1}M_{61}| \quad V_n = |(-1)^{6+2}M_{62}| \quad W_n = |(-1)^{6+3}M_{63}| \quad (24)$$

$$\Theta_n = |(-1)^{6+4}M_{64}| \quad \Phi_n = |(-1)^{6+5}M_{65}| \quad \Psi_n = |(-1)^{6+6}M_{66}|$$

where  $M_{6i}$  ( $i \rightarrow 1$  to  $6$ ) represent the minors of the elements  $A_{6i}$  for  $i \rightarrow 1$  to  $6$  of matrix  $[A]$ . The determinant of the co-factor elements presented in Equation. (24) gives us the final spatial solution for each coordinates of vibration. Since we have 12 roots for  $\alpha$ , subscript  $n$  is from 1 to 12. After obtaining  $\alpha$  in terms of  $\omega$  and obtaining the spatial solutions, the general solution of the coupled PDEs is expanded as follows.

$$\begin{pmatrix} u(x, t) \\ v(x, t) \\ w(x, t) \\ \theta(x, t) \\ \varphi(x, t) \\ \psi(x, t) \end{pmatrix} = \sum_{n=1}^{12} d_n \begin{pmatrix} U_n(\alpha = \alpha_n) \\ V_n(\alpha = \alpha_n) \\ W_n(\alpha = \alpha_n) \\ \Theta_n(\alpha = \alpha_n) \\ \Phi_n(\alpha = \alpha_n) \\ \Psi_n(\alpha = \alpha_n) \end{pmatrix} e^{\alpha_n x} e^{i\omega t} \quad (25)$$

Here,  $d_n$  is a solution constant for  $n \rightarrow 1$  to 12. The total of 12 boundary conditions are then used to find the frequencies using the algebraic equations below.

$$[L(\omega)]_{12 \times 12} \{\vec{d}\}_{12 \times 1} = \{0\}_{12 \times 1} \quad (26)$$

The non-trivial solution results in  $|L(\omega)| = 0$ , from which the natural frequencies are found.

### 3. Results and Discussions

Presented in this section are the natural frequencies and mode shapes for the cable-harnessed beam structure shown in Figure (1) using the analytical models developed in the previous section. The results are compared to the decoupled Euler Bernoulli model presented in Ref.[23] for the system parameters shown in Table (1). Further, the presented results help better understand the dynamics behind the coupling and its effects. In addition, sensitivity analysis such as the effects of the offset position, radius and pre-tension of the cable on the natural frequencies are further presented and discussed using the coupled Euler Bernoulli theory.

The position coordinates of the center of the cable in the  $y$  and  $z$  directions are given by the expressions  $y_c = \frac{b}{2} - r_c$ ;  $z_c = \frac{h}{2} + r_c$ . For the system parameters shown in Table (1), the values  $(y_c, z_c)$  are equal to  $(0.0043, 0.00145)$  m. The root of transcendental equation  $|L(\omega)| = 0$  is used to obtain the natural frequencies of the system for the parameters shown in Table (1) for the coupled system. Results of both Euler-Bernoulli and Timoshenko models are presented for parameters in Table (1). Fixed-fixed, cantilever and simply supported boundary conditions are considered. To validate the analytical results, a finite element analysis is performed. The system is discretized by assuming each displacement function to be a third order polynomial in  $x$  (where  $x$  is the length of the beam) [23,34]. The elemental mass and stiffness matrices are constructed from the strain and kinetic energy expressions using the Timoshenko model, Equations. (7-8). The structure was meshed into 200 elements. The total number of nodes in the system are 201 for all the boundary conditions considered. Once the elemental mass and stiffness matrices are constructed, they are assembled and respective boundary conditions are applied. The eigenvalue problem gives us the natural frequencies and the mode shapes. The natural frequency errors for each of the models in comparison with the FEA results are presented in the Tables. (2)-(4). To identify the coordinate of vibration associated with each frequency, the mode shapes are found and plotted in Figures. (2)-(4) in this paper and in Figures. (s1)-(s3) in the supplementary document. From this point, for referring figures and equations in the supplementary document, the format Figure. (s1) or Equation. (s1) will be used. For example, Figure. (s1) and Figure. (s2) represent the first and second figures in the supplementary document. The mass normalization condition for the coupled Timoshenko beam model can found by following the procedure outlined in [35].

$$\int_0^l (k_1 U_n(x)U_n(x) + k_2 V_n(x)V_n(x) + k_3 W_n(x)W_n(x) + k_4 \theta_n(x)\theta_n(x) + k_5 \varphi_n(x)\varphi_n(x) + k_6 \psi_n(x)\psi_n(x)) dx = 1 \quad (27)$$

Equation. (27) shows the mass normalization condition for a coupled Timoshenko model, the same condition can be easily obtained for an Euler-Bernoulli beam model and is shown in Equation. (28).

$$\int_0^l (k_1 U_n(x)U_n(x) + k_2 V_n(x)V_n(x) + k_3 W_n(x)W_n(x) + k_4 \theta_n(x)\theta_n(x)) dx = 1 \quad (28)$$

As an example, the first two mass-normalized mode shapes for the coupled theory using Euler-Bernoulli assumptions for several boundary conditions are shown in Figures. (2-4). The results in Figure. (2) for fixed-fixed boundary condition indicate that for the 1<sup>st</sup> and 2<sup>nd</sup> modes, the out-of-plane bending is the dominant mode. Similarly, the shapes for the in-plane bending, torsion-and axial dominant modes are presented in Figure. (s1) of the supplementary document. To further confirm, the dominance of each coordinate of vibration at a given frequency, a strain energy analysis is performed to find the contribution of each coordinate for the modes shown. Therefore, after obtaining the solution to the coupled PDEs, the

strain energy for each of the coordinates is calculated at each frequency. Finally, the percentages for the strain energy contributions of each of the coordinates of vibrations for each mode are plotted in Figure. (5a). These values indicate the dominance of each coordinate for a given mode, and further confirm the findings of Figure. (2) and Figure. (s1) of the supplementary document. The same explanation can be extended to cantilever and simply supported boundary conditions. It should be noted that the main assumption behind a decoupled model is that the stiffness values associated with the coordinates of vibrations not included in the analysis are infinitely large, and as a result those coordinates may be neglected. This leads to an overestimation of the frequencies using a decoupled model. Once the effects of these coordinates are included in the coupled analysis, the stiffness values associated with the previously ignored coordinates now become finite that result in a more reasonable natural frequency estimation and improved accuracy. The results shown in Tables. (2-4) further indicate the overestimation of the frequencies for the decoupled model as well as the improved accuracy for the coupled model that is particularly more important for the higher modes. In another words, the coupled model allows for the distribution of strain energy between coordinates of vibrations that is ignored in a decoupled analysis.

The mode shape results in Figure. (3) pertain to the cantilever boundary condition. For this boundary condition, it is shown that the out-of-plane bending is dominant in the first; whereas, the in-plane bending is dominant at the second mode. Also, from Figure (5b) and Figure (s2), the torsional mode is dominant at the fifth frequency, and the sixteenth mode corresponds to the first axial mode. For the simply supported boundary condition, Figure. (4), the out-of-plane bending is dominant in the first, second modes. From Figure. (s3) and Figure. (5c), In-plane bending is dominant in the mode 3. Torsion is dominant in the mode 6, and the mode 23 shown relates to the axial dominant mode.

The natural frequencies found using the decoupled and coupled models are presented and compared to the FEA results in Tables. (2-4). Comparing the errors in the natural frequency estimations for each of these methods clearly indicates the advantage of the coupled analysis over the decoupled. In particular, significant improvement in the accuracy can be observed for the out-of-plane bending dominant modes. It is shown that the decoupled model tends to overestimate the frequencies compared to the coupled model due to overestimating the overall stiffness of the system. This is because the decoupled model only allows for the out of plane bending, hence, it ignores the flexibility of the system in other directions and their vibrations. In addition, it can be seen that the Timoshenko model predicts the frequencies better when compared to the Euler Bernoulli. This is particularly noticeable for the higher in-plane bending modes due to the length to thickness ratio in that direction and the shear effects becoming more important.

Finally, to obtain more insight into the coupling effects, a sensitivity analysis is performed by varying several parameters such as radius of the cable, the offset position, and the tension in the cable. For simplicity, these analyses are performed using the coupled EB analytical model as the shear effects become

important for structures with larger length to thickness ratios. Figure. (6) shows, the effects of cable radius on natural frequencies for each mode while keeping other system parameters constant.

As the cable radius increases, the frequencies pertaining to the modes for which out of plane bending is dominant increase, while the frequencies for the dominantly torsional modes decrease. This is because the as the radius of the cable increases, the strain energy increases at a faster rate than the kinetic energy for the out of plane bending dominant mode and its frequency increases; however, the kinetic energy increases at a faster rate than the strain energy for the torsion dominant modes as the cable radius becomes larger, that results in smaller torsional frequencies.

In Figure (7), the errors between the natural frequencies of coupled and decoupled EB models compared to the FEA are plotted against the cable radius for different boundary conditions. As expected, when the cable radius increases, the coupling between different coordinates of vibrations gets stronger. It is shown that the error for the decoupled model with respect to the FEA becomes significantly larger when compared to the coupled model due to ignoring the coupling effects that are particularly important for larger cable radius values due to greater coupling.

The results for several cable-offset positions are presented in Figure (8). The natural frequency results shown in this figure further indicate the strain energy transfer between the in-plane and out-of-plane bending modes as the system coupling increases. As the cable is placed further from the center, the coupling effects are more pronounced that result in an energy transfer between the in-plane and out-of-plane bending modes subsequently causing the smaller frequencies for the out-of-plane bending dominant modes and larger frequencies for the in-plane modes. In addition, the frequency patterns show a symmetric behavior for offset positions on either side of the beam as expected.

To better understand the math behind this energy transfer, a further simplified model is built for the cable-harnessed beam in which only the coupled in-plane and out-of-plane bending modes are considered. Refs.[36,37] developed closed form expressions for natural frequencies of repeated truss structures and beams with initial loads. Following the same approach, closed form expressions for natural frequencies are obtained for the system in the following study for simply supported boundary conditions. The mathematical details for this procedure are explained below.

The reduced order Euler-Bernoulli model for the cable-harnessed beam that includes the bending modes only can be written as follows (reduced from Equations. (17a)-(17d)):

$$-k_2 \ddot{v} - b_2 v'''' - b_5 w'''' = 0 \quad (29a)$$

$$-k_3 \ddot{w} - b_3 w'''' - b_5 v'''' = 0 \quad (29b)$$

Simply supported boundary condition is considered as an example, therefore,

$$v = w = 0|_{x=0 \text{ or } l}$$

$$b_2 v'' + b_5 w'' = 0|_{x=0 \text{ or } l}$$

$$b_3 w'' + b_5 v'' = 0|_{x=0 \text{ or } l} \quad (30)$$

The last two expressions of Equation. (30) correspond to the equivalent bending moment in the in-plane and out-of-plane directions. Using the assumed form of solution for bending of a simply supported beam, we get,

$$\begin{aligned} v(x, t) &= V \sin\left(\frac{n\pi x}{l}\right) e^{i\omega t} \\ w(x, t) &= W \sin\left(\frac{n\pi x}{l}\right) e^{i\omega t} \end{aligned} \quad (31)$$

After substituting the general solution (Eq. (31)) in the coupled PDEs (Equations (29a) and (29b)), the simultaneous algebraic equations are converted into the matrix form and the frequency equation is obtained by setting the determinant of the resulting matrix to zero. The resulting natural frequency roots are as follows,

$$\begin{aligned} \omega_1 &= \sqrt{\frac{\frac{b_3 k_2 n^4}{l^4} + \frac{b_2 k_3 n^4}{l^4} - \frac{\sqrt{(b_3 k_2)^2 n^8 - 2b_2 b_3 k_2 k_3 n^8 + 4(b_5)^2 k_2 k_3 n^8 + (b_2 k_3)^2 n^8}}{l^4}}{2k_2 k_3}} \pi^2 \\ \omega_2 &= \sqrt{\frac{\frac{b_3 k_2 n^4}{l^4} + \frac{b_2 k_3 n^4}{l^4} + \frac{\sqrt{(b_3 k_2)^2 n^8 - 2b_2 b_3 k_2 k_3 n^8 + 4(b_5)^2 k_2 k_3 n^8 + (b_2 k_3)^2 n^8}}{l^4}}{2k_2 k_3}} \pi^2 \end{aligned} \quad (32)$$

The system parameters are assumed the same as Table. (1). The value of  $n$  is taken to be one. For  $n = 1$ , we get two frequencies from Equation (32). One of them corresponds to the out of plane bending dominant mode and the other corresponds to the in-plane dominant mode. As a result, the two natural frequencies obtained from Equation. (32) correspond to the same wavenumber. The detailed derivations to obtain Equation (32) and obtaining mode shapes corresponding to the frequency roots of Equation. (32) are presented in the supplementary document in the section S2. For the given wave number, the root with lower magnitude corresponds to the out-of-plane bending dominant mode and the root with higher magnitude corresponds to the in plane bending dominant mode. This can be confirmed from the mode shape plots Figures. (s4a) and (s4b) in the supplementary document.

Figure. (9) shows the variations for the strain energy and the fundamental natural frequency for these two bending modes as the cable offset changes. Zero offset in the plot denotes the system is decoupled at that point and at zero offset, the solutions pertaining to the decoupled system are presented. It is shown that as the offset distance increases, both the frequency and strain energy corresponding to the out-of-plane

bending dominant mode drop while they both increase for the in-plane bending mode. This indicates an energy transfer between the two modes as the coupling increases due to the offset position.

Another interesting aspect to study is the effect of the cable tension on the natural frequencies. In Figure. (s5) of supplementary document, the effect of cable pre-tension is studied on the natural frequencies of the cable-harnessed structure using the parameters given in Table. (1). Due to high bending stiffness, the structure is less susceptible to the effects of cable pre-tension. Therefore, to better study this effect, the system parameters in Table. (5) are additionally considered for a rectangular cross section. The position coordinates of the center of the cable ( $y_c, z_c$ ) are equal to (0.0098,0.00095) *m*. From Figure (10), we can see that as the cable pre-tension increases, the fundamental natural frequency for the out-of-plane bending drops to zero as the system undergoes buckling. As expected, the buckling load for the fixed-fixed boundary condition is the largest, then the simply supported, and finally the cantilever beam has the smallest critical loading. The strain energy distribution (bar graph) for beams with system parameters from Tables (1) and (5) for fixed-fixed boundary condition for the first mode (which corresponds to the out of plane bending dominant mode) are shown in Figures (11a) and (11b) respectively. In Figure (11a), the strain energy contributions from the axial, in-plane bending, out of plane bending and torsion coordinates are 5.08 %, 15.43 %, 79.48 % and 0.008 % respectively. In Figure (11b), the strain energy contributions in the axial, in-plane bending, out-of-plane bending and torsion coordinates are 0.005 %, 0.023 %, 71.75 % and 28.21 % respectively. As explained earlier for Figure (5a), in Figure (11a), the out of plane and in plane bending coordinates are strongly coupled to each other (for beam with parameters from Table (1)). In Figure (11b), the out of plane bending coordinate is strongly coupled to the torsion mode when compared to axial and in-plane bending as a beam with lower young's modulus and wider geometry is more flexible in the torsional direction. By increasing the value for the cable pre-tension, the system's coupling gets stronger that results in strain energy transfer between the out of plane bending mode and other coordinates of motion as shown in Figure (10). As similarly observed for the offset case study, for the modes associated with the same wave number, the mode with lower natural frequency transfers energy into the modes with the higher frequency. In this case, there is noticeable increase in the frequency for the torsion dominant mode when compared to the in-plane due to the nature of the coupling between these three modes. Similarly, the effect of cable pre-tension on a cable-harnessed structure with open-cross section is presented in Fig. (s7) of the supplementary document.

Finally, to clearly show the effect of coupling, a case study where forced excitation is applied to the structure in the out of plane bending direction and the resulting frequency response functions for the coupled Euler-Bernoulli analytical, coupled Timoshenko model, FEA and decoupled Euler Bernoulli model are presented in Figure (12).

The numerical parameters used are from Table. (1). The frequency response function for the coupled analytical model is calculated from Equation (33).

$$W(\omega) = \sum_{i=1}^{\infty} \frac{W(x = x_s). W(x = x_a)}{\omega_i^2 - \omega_f^2} \quad (33)$$

where  $W(x = x_s)$  represents the mass-normalized coupled out-of-plane bending displacement at the sensing location and  $W(x = x_a)$  represents the mass-normalized coupled out-of-plane bending displacement at the actuation location.  $\omega_f$  is the forcing frequency.  $\omega_i$  is the natural frequency corresponding to the mode  $i$ . Cantilever boundary condition is selected for this case study. The natural frequencies for cantilever condition are presented in Table. (3).

Here,  $x_s = 0.25 \text{ m}$  &  $x_a = 0.0952 \text{ m}$ , are the sensing and actuation locations respectively. Similarly, the frequency response functions for the decoupled and FEA models are calculated and plotted in Figure. (12). The significant peaks in the plots correspond to the out of plane bending direction and the first sharp peak corresponds to the in-plane bending dominant mode and the second sharp peak corresponds to the torsional dominant mode. As we can clearly observe from Figure. (12), the frequency response function of both coupled Euler-Bernoulli and coupled Timoshenko models match very well with that of FEA. The frequency response functions for the fixed-fixed and simply-supported boundary condition are presented in Figure. (s8) in the supplementary document. Therefore, the coupled model provides a better picture of the dynamics of the system when compared to a decoupled model.

#### 4. Conclusions

An analytical model is presented to study the free vibrations characteristics of a cable-harnessed beam structure motivated by space applications. A distributed parameter model that accounts for the effect of coupling in cable harnessed structures is developed. Kinetic and strain energy derivations are found using the Green-Lagrange strain field and Hamilton's principle is used to obtain both Timoshenko and Euler-Bernoulli coupled partial differential equations for the system. The natural frequencies obtained from the analytical model are validated against the finite element analysis results. The natural frequencies of the decoupled vibration model adopted in the literature were compared against the coupled vibration model used in this paper. The coupling effects between various coordinates of vibrations due to the presence of the cable are studied. The results demonstrate the importance of using a coupled vibration model to accurately predict the vibration behavior of the cable-harnessed structure. Several cable parameters are studied for their effects on the system's frequencies, coupling and the energy transfer between the modes.

It is observed that at larger cable radius, and if the cable is placed at an offset position, the coupling effect is greater and the coupled analytical model predicts the natural frequencies better than the decoupled model.

## Acknowledgments

The authors would like to thank Natural Sciences and Engineering Research Council under the Discovery Grant Program for supporting this research. They would also like to thank Dr. Blake Martin, a former graduate student in our group who worked on this research topic, for useful discussions.

## References

- [1] Coombs, D. M., Goodding, J. C., Babuška, V., Ardelean, E. V, Robertson, L. M., and Lane, S. A., 2011, “Dynamic Modeling and Experimental Validation of a Cable-Loaded Panel,” *Journal of Spacecraft and Rockets*, **48**(6), pp. 958–974.
- [2] Babuska, V., Coombs, D. M., Goodding, J. C., Ardelean, E. V, Robertson, L. M., and Lane, S. A., 2010, “Modeling and Experimental Validation of Space Structures with Wiring Harnesses,” *Journal of Spacecraft and Rockets*, **47**(6), pp. 1038–1052.
- [3] Goodding, J., Babuska, V., Griffith, D. T., Ingram, B., and Robertson, L., 2007, “Studies of Free-Free Beam Structural Dynamics Perturbations Due to Mounted Cable Harnesses,” *48th AIAA/ASME/ASCE/AHS/ASC Structures, Structural Dynamics, and Materials Conference*, p. 2390.
- [4] McClure, G., and Lapointe, M., 2003, “Modeling the Structural Dynamic Response of Overhead Transmission Lines,” *Computers & Structures*, **81**(8–11), pp. 825–834.
- [5] Spak, K., Agnes, G., and Inman, D., 2014, “Parameters for Modeling Stranded Cables as Structural Beams,” *Experimental Mechanics*, **54**(9), pp. 1613–1626.
- [6] Witz, J. A., and Tan, Z., 1992, “On the Axial-Torsional Structural Behaviour of Flexible Pipes, Umbilicals and Marine Cables,” *Marine Structures*, **5**(2–3), pp. 205–227.
- [7] Huang, S., 1999, “Stability Analysis of the Heave Motion of Marine Cable-Body Systems,” *Ocean Engineering*, **26**(6), pp. 531–546.
- [8] Robertson, L., Lane, S., Ingram, B., Hansen, E., Babuska, V., Goodding, J., Mimovich, M., Mehle, G., Coombs, D., and Ardelean, E., 2007, “Cable Effects on the Dynamics of Large Precision Structures,” *48th AIAA/ASME/ASCE/AHS/ASC Structures, Structural Dynamics, and Materials Conference*, p. 2389.
- [9] Goodding, J. C., Ardelean, E. V, Babuska, V., Robertson, L. M., and Lane, S. A., 2011, “Experimental Techniques and Structural Parameter Estimation Studies of Spacecraft Cables,” *Journal of Spacecraft and Rockets*, **48**(6), pp. 942–957.
- [10] Ardelean, E., Goodding, J., Coombs, D., Griffée, J., Babuška, V., Robertson, L., and Lane, S., 2010,

- “Cable Effects Study: Tangents, Rat Holes, Dead Ends, and Valuable Results,” *51st AIAA/ASME/ASCE/AHS/ASC Structures, Structural Dynamics, and Materials Conference 18th AIAA/ASME/AHS Adaptive Structures Conference 12th*, p. 2806.
- [11] Spak, K., Agnes, G., and Inman, D., 2014, “Cable Parameters for Homogenous Cable-Beam Models for Space Structures,” *Dynamics of Civil Structures, Volume 4*, Springer, pp. 7–18.
- [12] Spak, K. S., Agnes, G. S., and Inman, D. J., 2014, “Bakeout Effects on Dynamic Response of Spaceflight Cables,” *Journal of Spacecraft and Rockets*, **51**(5), pp. 1721–1734.
- [13] Spak, K. S., 2014, “Modeling Cable Harness Effects on Spacecraft Structures.” (Doctoral dissertation, Virginia Polytechnic Institute and State University).
- [14] Spak, K. S., Agnes, G. S., and Inman, D., 2013, “Towards Modeling of Cable-Harnessed Structures: Cable Damping Experiments,” *54th AIAA/ASME/ASCE/AHS/ASC Structures, Structural Dynamics, and Materials Conference*, p. 1889.
- [15] Choi, J., and Inman, D. J., 2014, “Spectrally Formulated Modeling of a Cable-Harnessed Structure,” *Journal of sound and vibration*, **333**(14), pp. 3286–3304.
- [16] Huang, Y.-X., Tian, H., and Zhao, Y., 2016, “Effects of Cable on the Dynamics of a Cantilever Beam with Tip Mass,” *Shock and Vibration*, **2016**.
- [17] Huang, Y.-X., Tian, H., and Zhao, Y., 2017, “Dynamic Analysis of Beam-Cable Coupled Systems Using Chebyshev Spectral Element Method,” *Acta Mechanica Sinica*, **33**(5), pp. 954–962.
- [18] Martin, B., and Salehian, A., 2013, “Cable-Harnessed Space Structures: A Beam-Cable Approach,” *24th International Association of Science and Technology for Development International Conference on Modelling and Simulation*, ACTA Press Calgary, AB, Canada, pp. 280–284.
- [19] Martin, B., and Salehian, A., 2013, “Dynamic Modelling of Cable-Harnessed Beam Structures with Periodic Wrapping Patterns: A Homogenization Approach,” *International Journal of Modelling and Simulation*, **33**(4), pp. 185–202.
- [20] Martin, B., and Salehian, A., 2013, “Vibration Analysis of String-Harnessed Beam Structures: A Homogenization Approach,” *54th AIAA/ASME/ASCE/AHS/ASC Structures, Structural Dynamics, and Materials Conference*, p. 1892.
- [21] Martin, B., and Salehian, A., 2014, “Vibration Modelling of String-Harnessed Beam Structures Using Homogenization Techniques,” *ASME 2014 International Mechanical Engineering Congress and Exposition*, American Society of Mechanical Engineers, p. V04BT04A074-V04BT04A074.
- [22] Martin, B., and Salehian, A., 2016, “Homogenization Modeling of Periodically Wrapped String-Harnessed Beam Structures: Experimental Validation,” *AIAA Journal*, pp. 3965–3980.
- [23] Martin, B., and Salehian, A., 2016, “Mass and Stiffness Effects of Harnessing Cables on Structural Dynamics: Continuum Modeling,” *AIAA Journal*, pp. 2881–2904.

- [24] Salehian, A., Cliff, E. M., and Inman, D. J., 2006, “Continuum Modeling of an Innovative Space-Based Radar Antenna Truss,” *Journal of Aerospace Engineering*, **19**(4), pp. 227–240.
- [25] Salehian, A., Inman, D. J., and Cliff, E. M., 2006, “Natural Frequency Validation of a Homogenized Model of a Truss,” *Proceedings of the XXIV-International Modal Analysis Conference*.
- [26] Salehian, A., Seigler, T. M., and Inman, D. J., 2007, “Dynamic Effects of a Radar Panel Mounted on a Truss Satellite,” *AIAA journal*, **45**(7), pp. 1642–1654.
- [27] Salehian, A., and Inman, D. J., 2008, “Dynamic Analysis of a Lattice Structure by Homogenization: Experimental Validation,” *Journal of Sound and Vibration*, **316**(1–5), pp. 180–197.
- [28] Salehian, A., and Inman, D. J., 2010, “Micropolar Continuous Modeling and Frequency Response Validation of a Lattice Structure,” *Journal of Vibration and Acoustics*, **132**(1), p. 11010.
- [29] Salehian, A., and Chen, Y., 2012, “On Strain-Rate Dependence of Kinetic Energy in Homogenization Approach: Theory and Experiment,” *AIAA journal*, **50**(10), pp. 2029–2033.
- [30] Stoykov, S., and Ribeiro, P., 2013, “Vibration Analysis of Rotating 3D Beams by the P-Version Finite Element Method,” *Finite Elements in Analysis and Design*, **65**, pp. 76–88.
- [31] Stoykov, S., and Margenov, S., 2014, “Nonlinear Vibrations of 3D Laminated Composite Beams,” *Mathematical Problems in Engineering*, **2014**.
- [32] Fonseca, J. R., and Ribeiro, P., 2006, “Beam P-Version Finite Element for Geometrically Non-Linear Vibrations in Space,” *Computer methods in applied mechanics and engineering*, **195**(9–12), pp. 905–924.
- [33] Stoykov, S., and Ribeiro, P., 2010, “Nonlinear Forced Vibrations and Static Deformations of 3D Beams with Rectangular Cross Section: The Influence of Warping, Shear Deformation and Longitudinal Displacements,” *International Journal of Mechanical Sciences*, **52**(11), pp. 1505–1521.
- [34] Tanaka, M., and Bercin, A. N., 1997, “Finite Element Modelling of the Coupled Bending and Torsional Free Vibration of Uniform Beams with an Arbitrary Cross-Section,” *Applied Mathematical Modelling*, **21**(6), pp. 339–344.
- [35] Song, O., Ju, J.-S., and Librescu, L., 1998, “Dynamic Response of Anisotropic Thin-Walled Beams to Blast and Harmonically Oscillating Loads,” *International Journal of Impact Engineering*, **21**(8), pp. 663–682.
- [36] Stephen, N. G., and Zhang, Y., 2006, “Coupled Tension–torsion Vibration of Repetitive Beam-like Structures,” *Journal of sound and vibration*, **293**(1–2), pp. 253–265.
- [37] Vörös, G. M., 2009, “On Coupled Bending–torsional Vibrations of Beams with Initial Loads,” *Mechanics Research Communications*, **36**(5), pp. 603–611.

## List of Figures

**Fig 1:** Representation of the cable harness beam along with the coordinate axes.

**Fig 2:** Vibrations mode shapes for fixed-fixed boundary conditions using coupled EB theory for the first two modes.

**Fig 3:** Vibrations mode shapes for cantilever boundary conditions using coupled EB theory for the first two modes.

**Fig 4:** Vibrations mode shapes for simply supported boundary conditions using coupled EB theory for the first two modes.

**Fig 5:** Percentage for the strain energy contribution of each modal coordinate with respect to mode number.

**Fig 6:** Effects of cable radius on the coupled natural frequencies.

**Fig 7:** Error comparisons for natural frequencies between the coupled and decoupled models and the FEA.

**Fig 8:** Effect of cable offset position on the coupled natural frequencies.

**Fig 9:** Strain energy and natural frequency with respect to cable offset position.

**Fig 10:** Effect of cable pre-tension on the natural frequencies for first in-plane bending, out-of-plane bending and torsional mode using the system parameters of Table. (5).

**Fig 11** Bar graph of strain energy contributions for mode 1 for beam with parameters from a) Table 1 b) Table 5 for fixed-fixed boundary condition.

**Fig 12:** Frequency response function for cantilever boundary condition.

## List of Tables

**Table 1:** Material and geometrical properties of the cable harnessed beam structure.

**Table 2:** Natural Frequencies for coupled and decoupled models for fixed-fixed boundary conditions (Hz)

**Table 3:** Natural Frequencies for coupled and decoupled models for cantilever boundary conditions (Hz)

**Table 4:** Natural Frequencies for coupled and decoupled models for simply supported boundary conditions (Hz).

**Table 5:** Material and geometrical properties for the tension case study, rectangular cross-section beam.

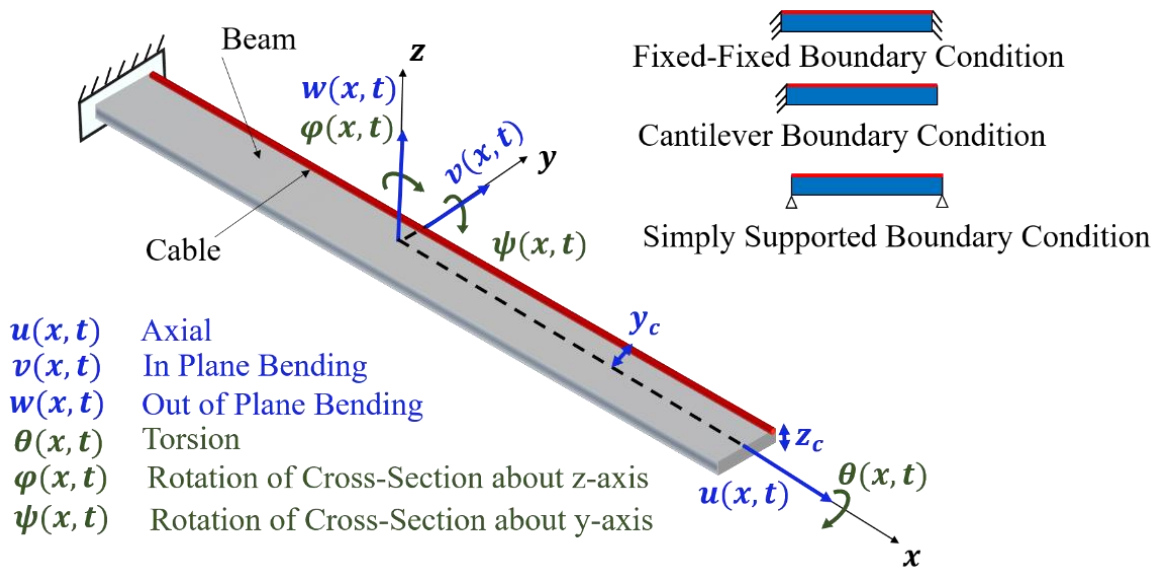


**Fig 1:** Representation of the cable harness beam along with the coordinate axes.

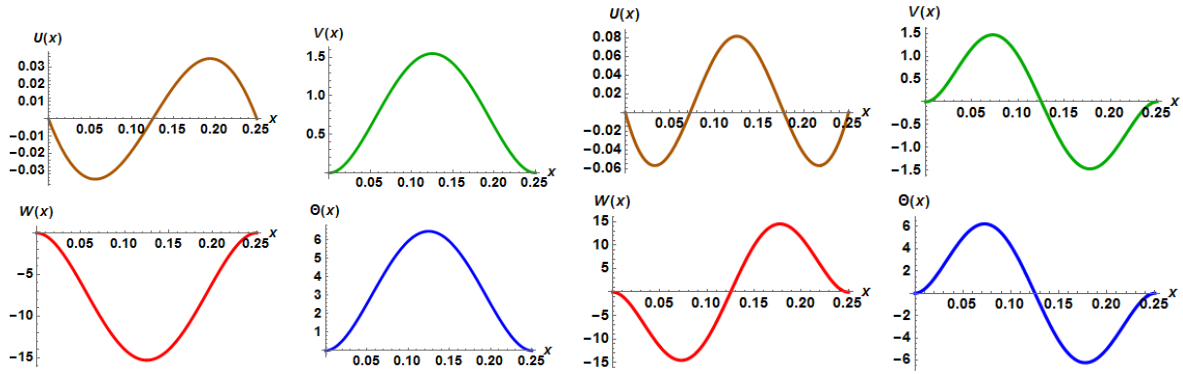


**Fig 2:** Vibrations mode shapes for fixed-fixed boundary conditions using coupled EB theory for the first two modes

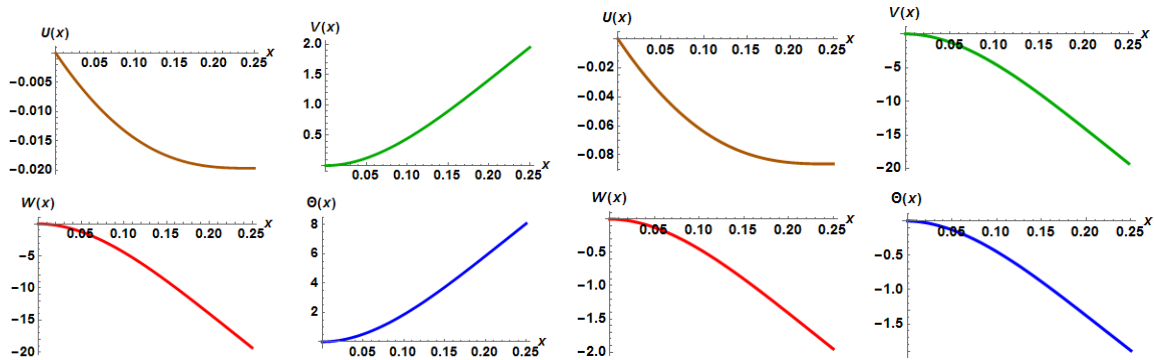


**Fig 3:** Vibrations mode shapes for cantilever boundary conditions using coupled EB theory for the first two modes

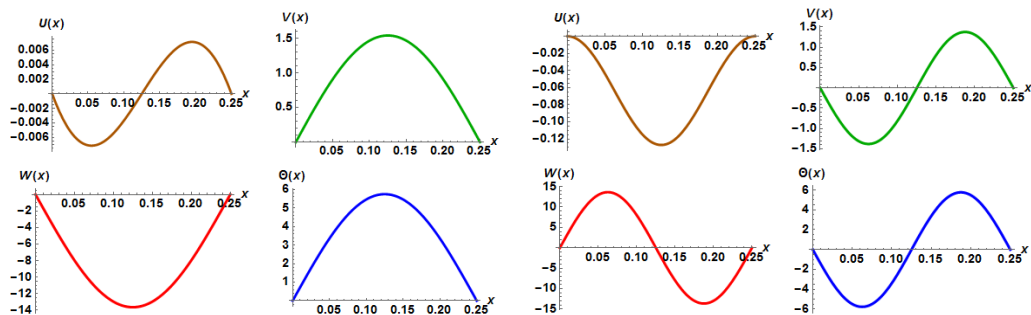


**Fig 4:** Vibrations mode shapes for simply supported boundary conditions using coupled EB theory for the first two modes

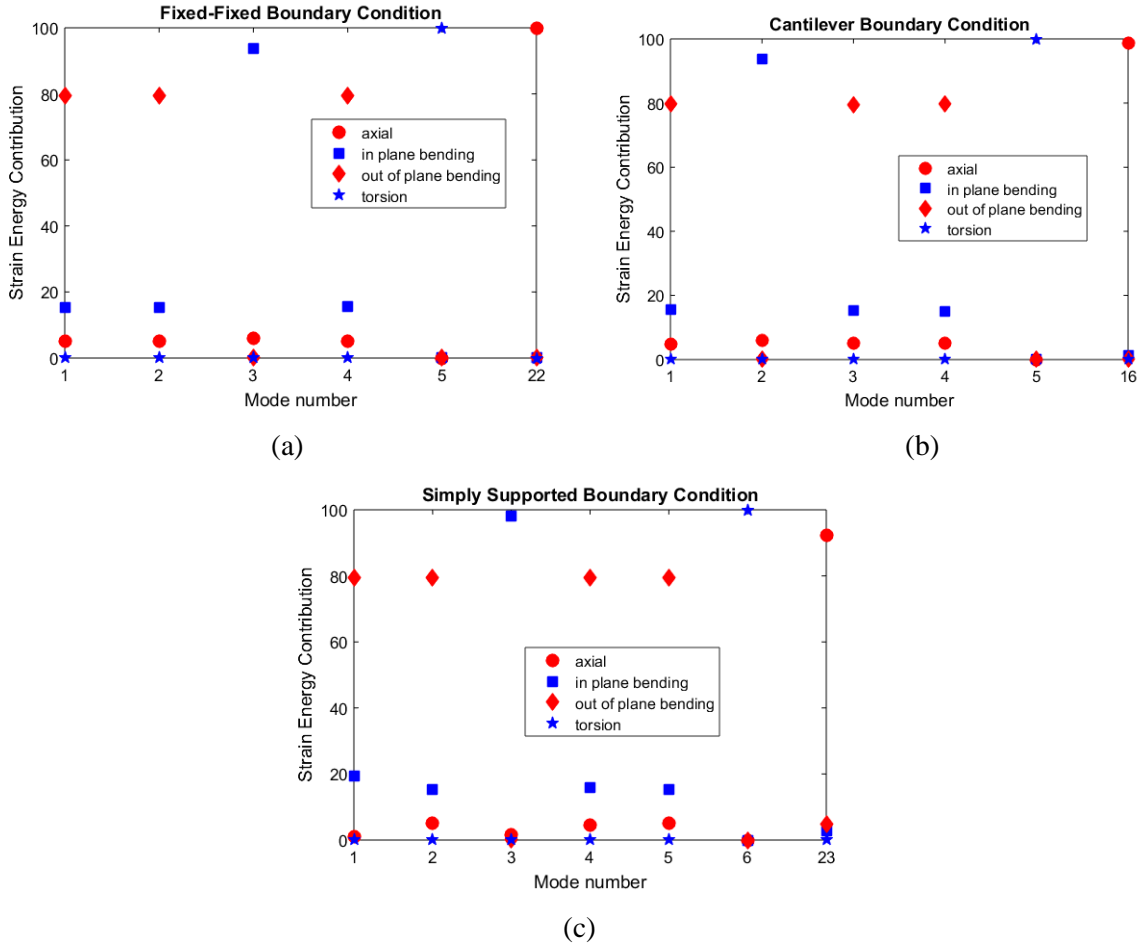
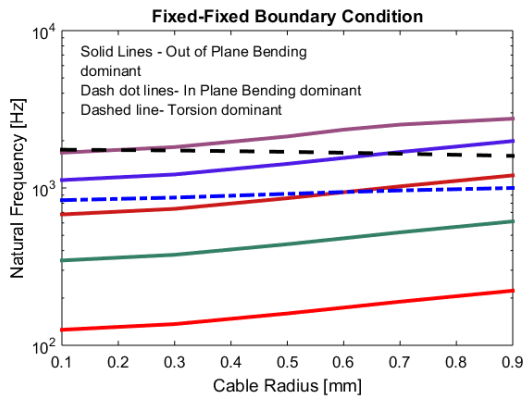
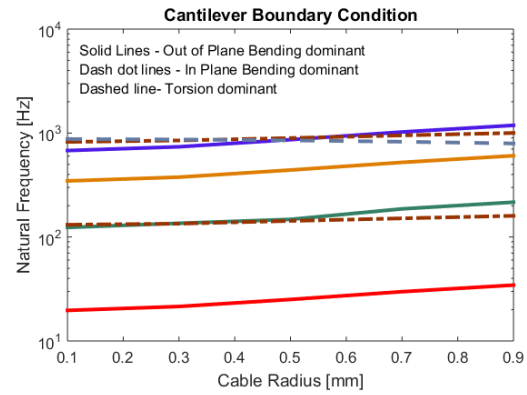


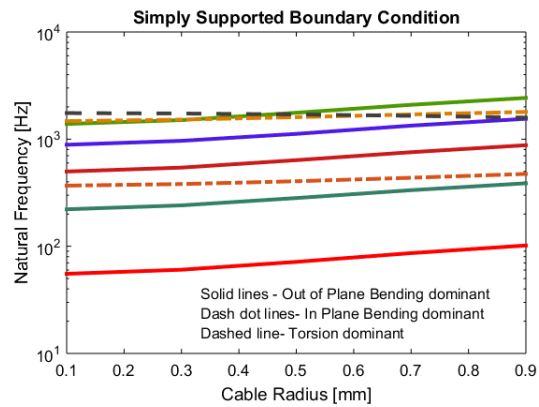
**Fig 5:** Percentage for the strain energy contribution of each modal coordinate with respect to mode number



(a)

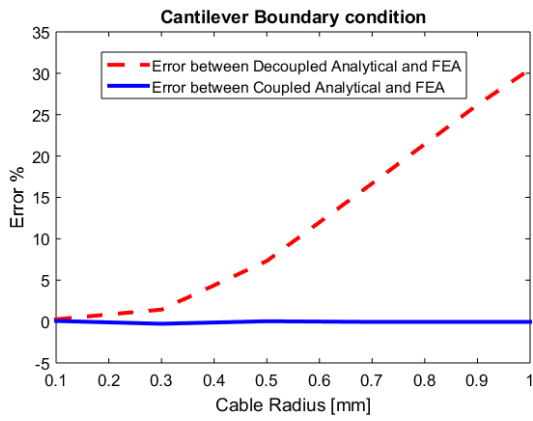


(b)

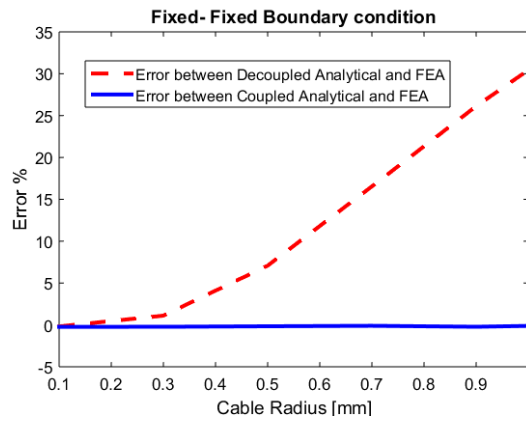


(c)

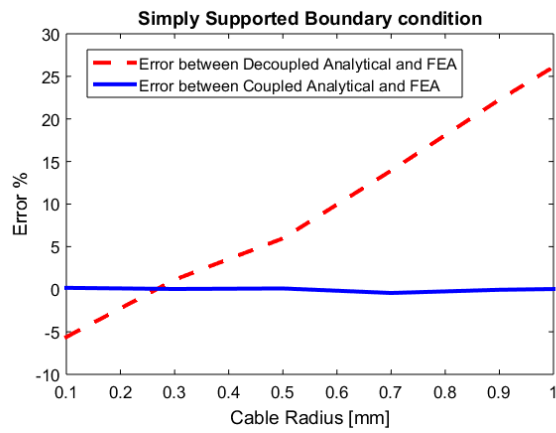
**Fig 6:** Effects of cable radius on the coupled natural frequencies



(a)

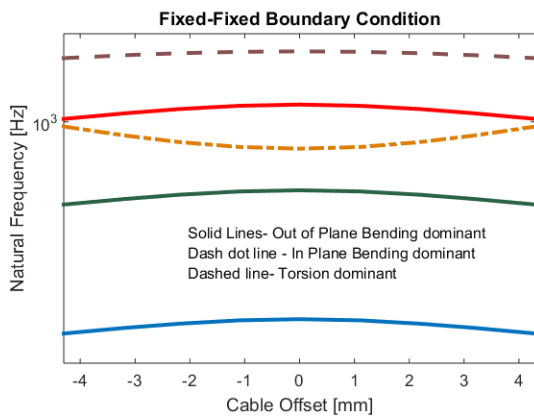


(b)

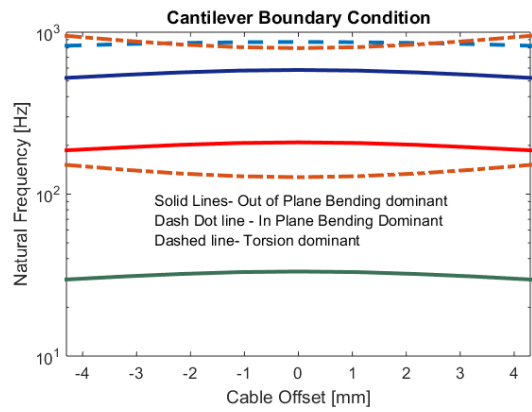


(c)

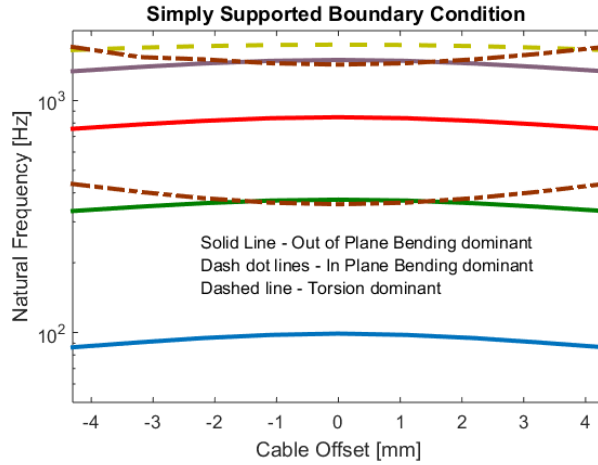
**Fig 7:** Error comparisons for natural frequencies between the coupled and decoupled models and the FEA



(a)

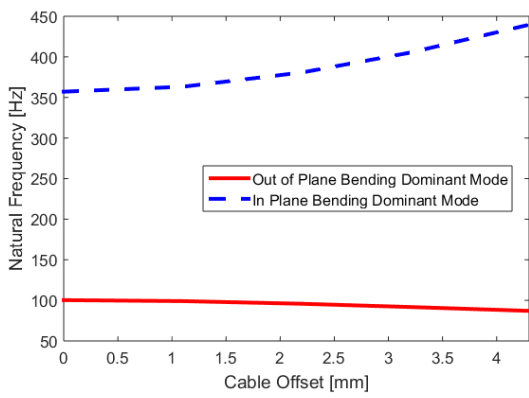


(b)

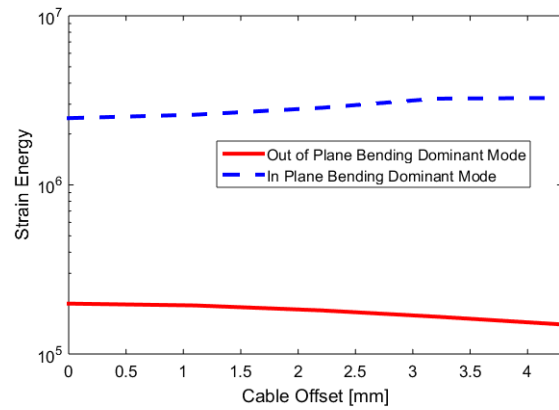


(c)

**Fig 8:** Effect of cable offset position on the coupled natural frequencies



(a)



(b)

**Fig 9:** Strain energy and natural frequency with respect to cable offset position

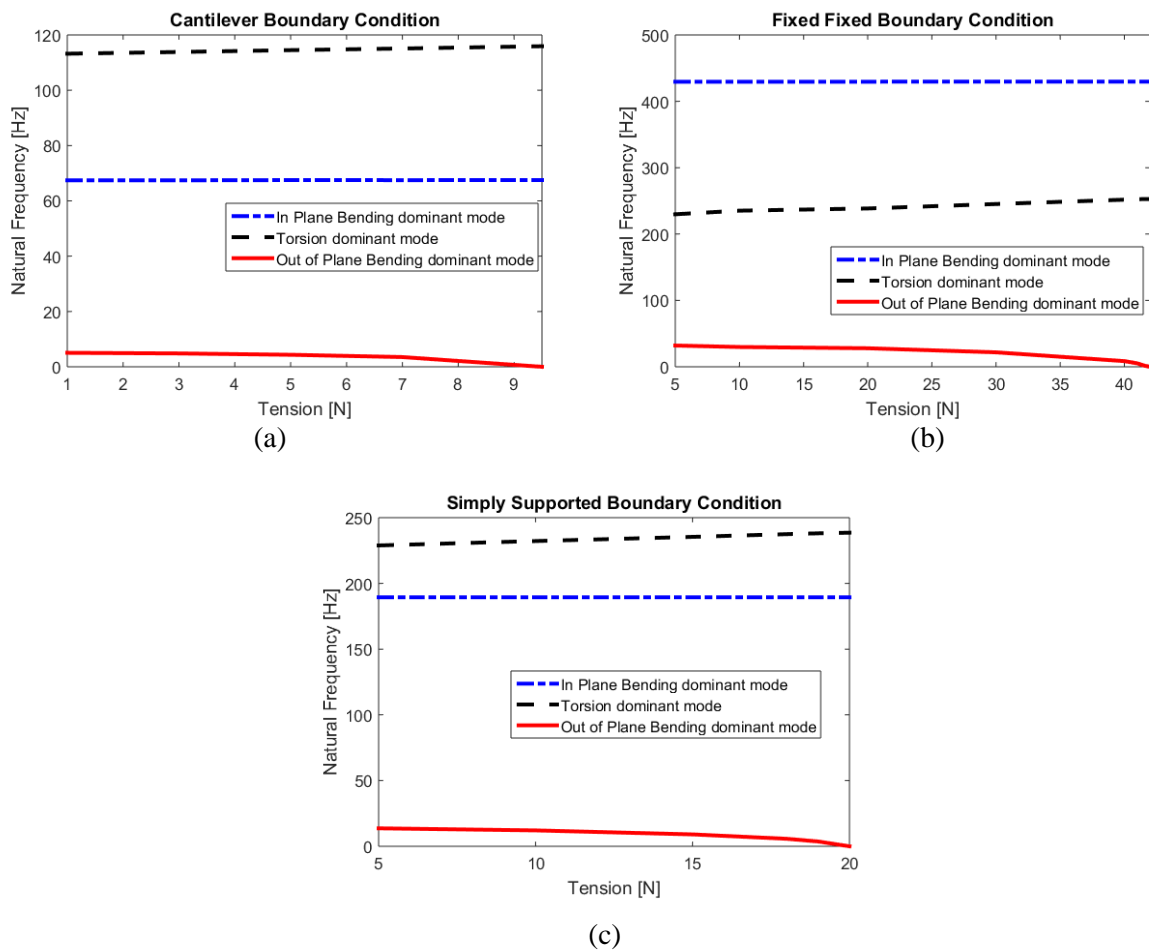
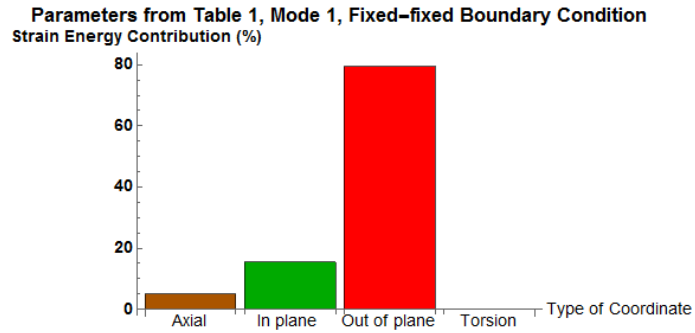
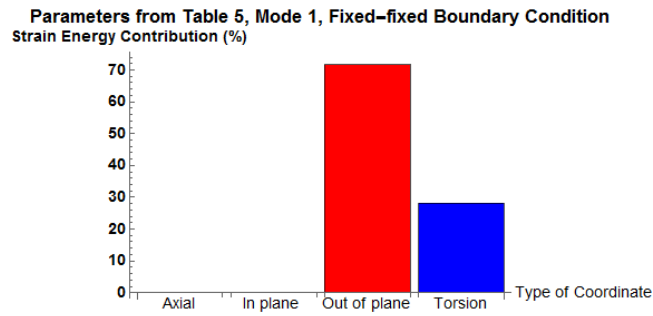


**Fig 10:** Effect of cable pre-tension on the natural frequencies for first in-plane bending, out-of-plane bending and torsional mode using the system parameters of Table (5)



(a)



(b)

**Fig 11:** Bar graph of strain energy contributions for mode 1 for beam with parameters from a) Table 1 b) Table 5 for fixed-fixed boundary condition.

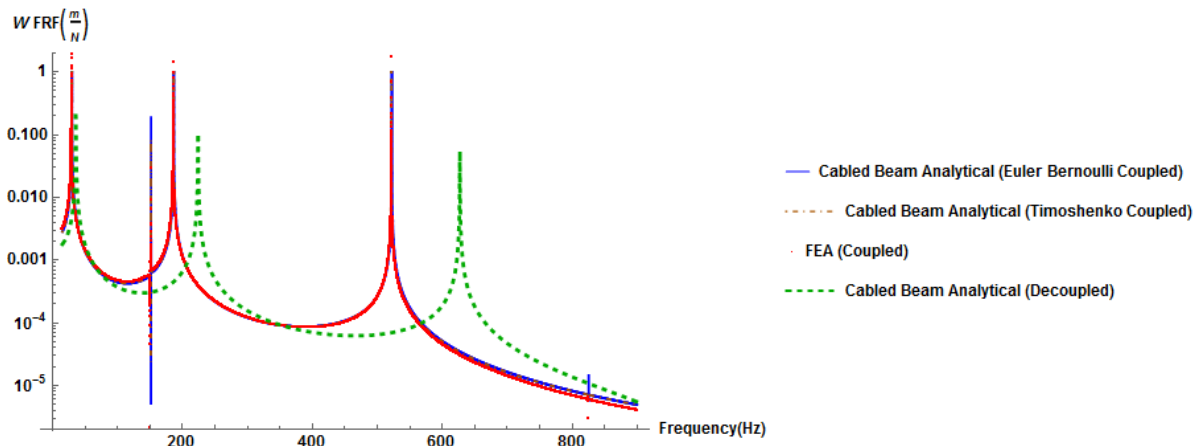


**Fig 12:** Frequency response functions for Cantilever boundary condition.

**Table 1:** Material and geometrical properties of the cable harnessed beam structure.

<b>System parameters</b>	<b>Value</b>
Beam length ( $l$ )	0.25 m
Beam width ( $b$ )	0.01 m
Beam height ( $h$ )	0.0015 m
Beam density ( $\rho_b$ )	2,700 Kg/m <sup>3</sup>
Beam modulus of elasticity ( $E_b$ )	68.9 GPa
Beam Shear modulus ( $G_b$ )	26 GPa
Beam Poisson's ratio ( $\nu$ )	0.34
Cable tension ( $T$ )	25 N
Cable radius ( $r_c$ )	0.0007 m
Cable density ( $\rho_c$ )	1,400 Kg/m <sup>3</sup>
Cable modulus of elasticity ( $E_c$ )	150 GPa

**Table 2:** Natural Frequencies for coupled and decoupled models for fixed-fixed boundary conditions (Hz)

Mode	Decoupled Euler-Ber.	Coupled Euler-Ber.	Coupled Timoshenko	FEA	Error % Decoupled	Error % Coupled Euler-Ber.	Error % Coupled Timoshn ko
1	227.36 OP	189.39	189.23	189.75	16.53	-0.16	-0.22
2	626.73 OP	521.87	521.55	522.68	16.60	-0.13	-0.18
3	990.1 IP	964.32	949.51	952.35	3.81	1.20	-0.28
4	1228.6 OP	1023.7	1020.98	1023.63	16.68	0.00	-0.21
5	1650.8 T	1650.8	1650.44	1652.8	-0.12	-0.12	-0.14
6	2031 OP	1691.8	1685.45	1689.91	16.79	0.09	-0.21
7	3034 OP	2527.4	2513.06	2520.45	16.92	0.22	-0.24
8	2729.3 IP	2657.9	2567.17	2576.83	5.58	2.97	-0.35
9	3301.7 T	3301.7	3302.47	3305.59	-0.11	-0.11	-0.09
10	4237.6 OP	3528.5	3504.59	3513.78	17.08	0.34	-0.21
22	10889 A	10890	10886.2	10900.1	-0.10	-0.09	-0.12

\*OP, IP, T and A refer to the out-of-plane bending, in-plane bending, torsional and axial modes respectively.

**Table 3:** Natural Frequencies for coupled and decoupled models for cantilever boundary conditions (Hz)

Mode	Decoupled Euler-Ber.	Coupled Euler-Ber.	Coupled Timoshenko	FEA	Error % Decoupled	Error % Coupled Euler-Ber.	Error % Coupled Timoshe- nko
1	35.72 OP	29.79	29.63	29.76	16.67	0.07	-0.37
2	155.58 IP	151.53	151.32	151.47	2.63	0.03	-0.09
3	223.91 OP	186.53	186.37	186.65	16.63	-0.05	-0.12
4	626.86 OP	522.35	521.71	522.38	16.66	-0.00	-0.10
5	825.42 T	825.38	825.69	825.91	-0.05	-0.06	-0.02
6	975.07 IP	949.52	938.53	939.92	3.60	0.98	-0.14
7	1228.5 OP	1023.7	1021.46	1022.75	16.74	0.07	-0.10
8	2031 OP	1691.8	1687.04	1688.65	16.85	0.15	-0.07
9	2476.3 T	2476.5	2476.45	2477.73	-0.05	-0.04	-0.05
10	2729.8 IP	2527.4	2516.24	2518.81	7.72	0.31	-0.09
16	5444.5 A	5447.9	5446.28	5449.63	-0.09	-0.03	-0.06

\*OP, IP, T and A refer to the out-of-plane bending, in-plane bending, torsional and axial modes respectively.

**Table 4:** Natural Frequencies for coupled and decoupled models for simply supported boundary conditions (Hz)

Mode	Decoupled Euler-Ber.	Coupled Euler-Ber.	Coupled Timoshenko	FEA	Error % Decoupled	Error % Coupled Euler-Ber.	Error % Coupled Timoshe nko
1	100.29 OP	86.38	86.34	86.32	13.93	0.06	0.01
2	401.18 OP	334.06	334.06	334.03	16.73	0.00	0.00
3	436.76 IP	436.40	434.65	434.98	0.40	0.32	-0.07
4	902.67 OP	755.34	754.07	754.17	16.45	0.13	-0.01
5	1604.75 OP	1336.58	1333.56	1333.87	16.88	0.16	-0.01
6	1650.84 T	1650.44	1650.44	1652.8	-0.11	-0.14	-0.14
7	1747.06 IP	1701.37	1675.90	1677.3	3.99	1.37	-0.08
8	2507.42 OP	2091.3	2083.34	2084.66	16.86	0.26	-0.05
9	3610.69 OP	3008.03	2992.11	2992.51	17.12	0.42	-0.01
10	3301.69 T	3302.47	3302.47	3305.59	-0.11	-0.09	-0.09
23	10889.0 A	10797.1	10766.8	10783.9	0.96	0.12	-0.15

\*OP, IP, T and A refer to the out-of-plane bending, in-plane bending, torsional and axial modes respectively.

**Table 5:** Material and geometrical properties for the tension case study, rectangular cross-section beam.

<b>System parameters</b>	<b>Value</b>
Beam length	0.25 m
Beam width	0.02 m
Beam height	0.0015 m
Beam density	1,300 Kg/m <sup>3</sup>
Beam modulus of elasticity	2.2 GPa
Beam shear modulus	0.785 GPa
Beam Poisson's ratio	0.4
Cable radius	0.0002 m
Cable density	1,200 Kg/m <sup>3</sup>
Cable modulus of elasticity	2 GPa